Int. Journal of Refractory Metals and Hard Materials 51 (2015) 137–140

Contents lists available at ScienceDirect

Int. Journal of Refractory Metals and Hard Materials

journal homepage: www.elsevier.com/locate/IJRMHM

Thermodynamic analysis and reduction of tungsten trioxide using methane

S. Cetinkaya *, S. Eroglu

Istanbul University, Engineering Faculty, Department of Metallurgical and Materials Eng., Avcilar, 34320 Istanbul, Turkey

ARTICLE INFO

Article history:
Received 16 February 2015
Received in revised form 19 March 2015
Accepted 23 March 2015
Available online 25 March 2015

Keywords:
Oxide reduction
Methane
Tungsten
Chemical vapor transport
Thermodynamic analysis

ABSTRACT

The present study aims to investigate reduction behavior of WO_3 using pure CH_4. Prior to the experiments, equilibrium thermodynamic analysis in the WO_3–CH_4 system was carried out by the method of minimization of Gibbs' free energy. The analysis indicates that WO_3 can be reduced to metallic W by CH_4 at temperatures above ~1150 K. The experiments were carried out at 1200, 1250 and 1300 K in a flowing pure CH_4 atmosphere. Mass measurements and X-ray diffraction technique were used to characterize the products at various stages of reactions. It was found that the extent of the reduction of WO_3 increased with time and temperature. Experimental and thermodynamic results showed that W is obtained from WO_2 which is an intermediate product formed by the reactions between WO_3 and CH_4. Carburization was observed after the oxide reduction was completed at the temperatures studied. Single phase W product was obtained within 10 min at 1300 K. FEG-SEM analysis on the sample prepared at this condition yielded fine round particles and coarse particles with facets. Possible reaction mechanisms for the formation of W in the W–O–C–H system were elucidated using thermodynamic and experimental results. It was demonstrated that CH_4 acts as a reducing agent for WO_3.

1. Introduction

Tungsten, also known as wolfram, has superior properties such as high density, high melting point, high modulus of elasticity, high hardness, high strength, low thermal expansion, low vapor pressure and good corrosion resistance. Owing to these properties, it is used as a major constituent for various parts such as radiation shields, heating elements, kinetic energy penetrators, and balance weights. Furthermore, it is also used for the production of tungsten carbide (WC) which is an important component of wear resistant parts (e.g. cutting tools, dies, nozzles).

Tungsten oxide is conventionally used for tungsten production. Primary sources for tungsten oxide are wolframite ($(Fe,Mn)WO_4$) or scheelite ($CaWO_4$) ores. Tungsten-containing scrap materials are also used as secondary source. These sources are used to initially obtain tungsten oxide by hydro/pyrometallurgical processes. Tungsten oxide is then thermally reduced mainly by hydrogen to form metallic tungsten [1]. Hydrogen (H_2) is widely employed for the reduction of metal oxides. But, it is relatively an expensive reducing agent. Methane (CH_4) has been recently used as an alternative reducing agent to obtain metallic Zn [2], Co [3], Ni [4] and Sn [5] from ZnO, CoO, NiO and SnO_2 because it is relatively cheap and abundant (a main component of natural gas).

To the best of our knowledge, no report has been published on the synthesis of tungsten by reduction of WO_3 with CH_4. The present study aims to investigate pyrometallurgical reduction behavior of WO_3 in a flowing CH_4 atmosphere. Furthermore, thermodynamic analysis in the WO_3–CH_4 system was carried out in order to get a deeper insight into the thermochemistry of the process.

2. Thermodynamic analysis

Thermodynamic analysis is a useful tool to predict the process parameters that yield the desired phases and to understand material synthesis processes. The analysis has been carried out by the method of minimization of the Gibbs' free energy of a system [6]. For a system of known input composition, it computes both the equilibrium gas phase and condensed phase compositions at a given pressure and temperature. The calculation requires specifying all possible species and condensed phases known to exist in the temperature range of interest. In the present study, WO_3 and CH_4 were used as reactants for W synthesis. Therefore, equilibrium calculations were carried out in the W–O–C–H system. In this system, 46 species were considered to be as the constituents of the gas phase. They include CH_4, CH_3, C_2H_6, C_2H_4, CH_2O, CO, CO_2, H_2, H_2O and $WO_2(OH)_2$. Condensed equilibrium phases were assumed to be WO_3, WO_2, W, W_2C, WC and C. Non-stoichiometric tungsten oxides (such as $WO_{2.9}$ and $WO_{2.72}$) were excluded from the calculations for the sake of clarity. Input thermodynamic data in the form of Gibbs' free energy of the formation of the constituents were obtained from the thermochemical tables [7,8]. Thermodynamic calculations of the complex equilibria were performed using a modified version of Eriksson's computer program SOLGASMIX [9]. Equilibrium stability diagram for condensed phases was computed as a function of temperature

* Corresponding author.
E-mail address: senol-c@istanbul.edu.tr (S. Cetinkaya).

http://dx.doi.org/10.1016/j.ijrmhm.2015.03.017
0263-4368/

(1000–1500 K) and input CH_4 mole fraction (X_{CH_4}) at 1 atm. X_{CH_4} is defined as $n^\circ_{CH_4} / (n^\circ_{CH_4} + n^\circ_{WO_3})$ where n° represents the initial number of moles of CH_4 and WO_3. The calculated results are shown in Fig. 1. The information obtained from this figure can be summarized as follows. $WO_3 + WO_2$, WO_2, $WO_2 + W$, $WO_2 + WC$, $WO_2 + W + WC$, W, $W + WC$, WC and $WC + C$ phase fields are seen from the diagram. The figure also reveals that single W phase (the desired phase) forms at temperatures above ~1150 K and W phase field widens with increasing temperature. For example, CH_4 mole fractions predicted for single phase W formation are limited to 0.606 at 1150 K, 0.576–0.718 at 1300 K and 0.548–0.746 at 1500 K. WC and free C phases appear successively as X_{CH_4} increases above the upper limits. Equilibrium analysis indicates that WO_3 can be reduced to metallic W by CH_4 at temperatures above 1150 K. Hence, the reduction experiments were carried out at temperatures higher than 1150 K.

3. Experimental procedures

The experimental set-up used for the present study essentially consists of a hot-wall furnace with SiC heating elements, a quartz tube (20 mm in diameter, 500 mm in length) and gas flow meters. The chemicals used for the present study were Ar (99.999%), CH_4 (99.5%) and WO_3 (≥99.5%) powder. Particle size of the oxide powder used was reported to be <100 nm by the producer (Sigma-Aldrich).

An alumina boat with gas entrance side cut to allow smooth gas flow was loaded with ~200 mg WO_3 powder. Moisture in the oxide powder was removed at 373 K in an oven prior to the experiments. The oxide powder was heated at a rate of ~25 K/min in a flowing Ar atmosphere (85 standard cm^3/min, sccm) to 1200, 1250 and 1300 K. When these temperatures were reached, Ar flow was stopped and CH_4 was then allowed to flow into the system at a rate of 40 sccm for various periods of times. The reaction products were allowed to cool to room temperature in Ar flow (85 sccm). Mass measurements before and after the experiments were carried out by a calibrated electronic balance with a sensitivity of $\pm 10^{-4}$ g in order to determine the extent of the reactions. Mass change (%) was calculated using the formula of $((m_f - m_o) / m_o) \times 100$ where m_f and m_o are the final mass of the products and original mass of the oxide powder (WO_3), respectively.

A parafocusing X-ray diffractometer (XRD) equipped with a Cu radiation tube ($\lambda_{K\alpha} = 0.15418$ nm) was employed for the phase analysis. A Field Emission Gun Scanning Electron Microscope (FEG-SEM) was employed to reveal powder morphologies.

4. Results and discussion

4.1. Characterization of the starting oxide powder

Fig. 2 shows the X-ray diffraction pattern and SEM image of the tungsten oxide powder used for the present study. As can be seen from figure, the diffraction angles and intensities of the peaks are in agreement with those of standard WO_3 (PDF No 04-05-4301) shown as a line pattern in the figure. This indicates that the starting powder is stoichiometric WO_3. The broad diffraction peaks observed are attributed to fine particles. The inset in Fig. 2 shows that the powder used consists of nearly round particles. Mean particle size of the powder was determined to be 28 ± 7 nm using the SEM image.

4.2. Reduction of tungsten trioxide

4.2.1. Mass changes

Fig. 3 shows change in the sample mass as a function reaction temperature and time. The information obtained from this figure can be summarized as follows. The sample mass decreases rapidly at the early stage of the reaction for all the temperatures studied owing to oxygen loss from WO_3. This stage was followed by mass gain as the reaction time increases. In addition, the mass loss rate increases with the reaction temperature. Among the samples obtained, the highest mass losses were observed to be 17.98%, 17.86% and 20.86% at the reaction times of 90, 25 and 10 min for 1200, 1250 and 1300 K, respectively. Horizontal dashed line at 20.70% in the figure shows the theoretical mass loss calculated for the reduction of WO_3 to W. Comparison of the theoretical value with the highest mass loss data implies that the significant reduction takes place in CH_4 atmosphere at the temperatures studied. It should be noted that the highest mass loss at 1300 K is close to the theoretical one. This suggests that almost full reduction takes place within 10 min at 1300 K. The highest mass loss data at 1200 and 1250 K are observed to be above the theoretical one, implying incomplete reduction of the oxide and/or carbon uptake by powder. Mass gain observed beyond the highest mass loss times can be solely attributed to C uptake by the powder as a result of methane pyrolysis at the temperatures studied, as no oxide phases were revealed by the XRD patterns of the samples with the highest mass loss (Fig. 4).

4.2.2. Phase analyses

Fig. 4 shows the XRD patterns of the samples with the highest mass losses obtained at 1200, 1250 and 1300 K for the reaction times of 90, 25 and 10 min, respectively. Also, the XRD pattern of the sample prepared at 1300 K for 5 min was included in the figure in order to reveal the phases at the early stage of reduction. The line patterns of the matched materials published by JCPDS are also displayed in the figure. As seen from the figure, all the patterns display intense diffraction peaks (marked by •) at 40.3°, 58.3° 73.2° and 87.0°. Interplanar spacings associated with these peaks were calculated to be 0.2238, 0.1583, 0.1293 and 0.1120 nm. These peaks were assigned to the (110), (200), (211) and (220) crystal planes of BCC W (PDF No 00-004-0806) because the interplanar spacings are found to be in fairly good agreement with the published standard values (0.2238, 0.1582, 0.1292 and 0.11188 nm). The peak intensities also agreed with those of the standard diffraction file for W. It is noticed from the patterns that there are other phases

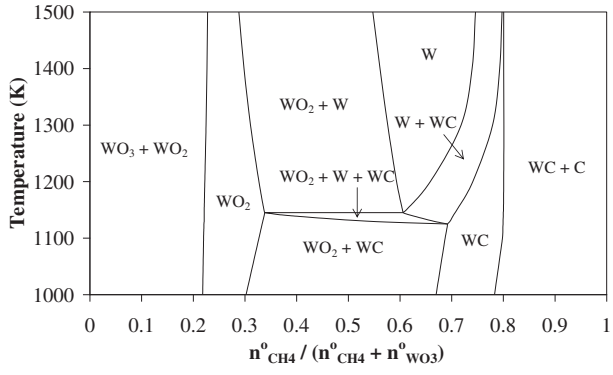

Fig. 1. Equilibrium stability diagram showing condensed phase fields as a function of temperature and input CH_4 mole fraction (X_{CH_4}) in the WO_3–CH_4 system at 1 atm.

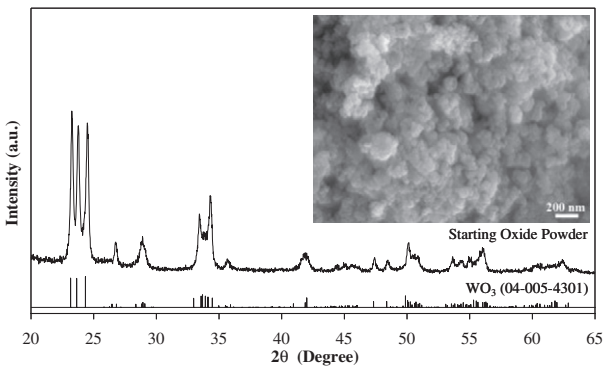

Fig. 2. XRD pattern and SEM image of the starting oxide powder (WO_3).